

# We are IntechOpen, the world's leading publisher of Open Access books Built by scientists, for scientists

6,900

Open access books available

186,000

International authors and editors

200M

Downloads

Our authors are among the

154

Countries delivered to

TOP 1%

most cited scientists

12.2%

Contributors from top 500 universities



WEB OF SCIENCE™

Selection of our books indexed in the Book Citation Index  
in Web of Science™ Core Collection (BKCI)

Interested in publishing with us?  
Contact [book.department@intechopen.com](mailto:book.department@intechopen.com)

Numbers displayed above are based on latest data collected.  
For more information visit [www.intechopen.com](http://www.intechopen.com)



# Nanowires Integrated to Optical Waveguides

*Ricardo Téllez-Limón and Rafael Salas-Montiel*

## Abstract

Chip-scale integrated optical devices are one of the most developed research subjects in last years. These devices serve as a bridge to overcome size mismatch between diffraction-limited bulk optics and nanoscale photonic devices. They have been employed to develop many on-chip applications, such as integrated light sources, polarizers, optical filters, and even biosensing devices. Among these integrated systems can be found the so-called hybrid photonic-plasmonic devices, structures that integrate plasmonic metamaterials on top of optical waveguides, leading to outstanding physical phenomena. In this contribution, we present a comprehensive study of the design of hybrid photonic-plasmonic systems consisting of periodic arrays of metallic nanowires integrated on top of dielectric waveguides. Based on numerical simulations, we explain the physics of these structures and analyze light coupling between plasmonic resonances in the nanowires and the photonic modes of the waveguides below them. With this chapter we pretend to attract the interest of research community in the development of integrated hybrid photonic-plasmonic devices, especially light interaction between guided photonic modes and plasmonic resonances in metallic nanowires.

**Keywords:** plasmonics, integrated optics, nanowires, optical waveguides, hybrid modes

## 1. Introduction

Plasmonics, the science of plasmons, is a research field that has been extensively studied in recent years due to its multiple applications like biosensing, optical communications, or quantum computing, to mention but a few.

Generally, the field of plasmonics is associated with two types of collective oscillations of conductive electrons at the boundaries of metallic nanostructures, known as surface plasmon polaritons (SPP) and localized surface plasmons (LSP). While SPP are referred as surface waves propagating at a dielectric-metal interface, LSP can be regarded as standing surface waves confined in metallic nanoparticles embedded in a dielectric environment [1].

As it is well known, SPP modes can only be excited when appropriate phase match conditions are fulfilled. An option to achieve this condition, is by making use of the electromagnetic near field scattered by a local defect or emitter. To this purpose, the LSP mode of a metallic nanoparticle can be excited and coupled to the SPP of a metallic substrate, giving rise to hybrid plasmon polaritons [2, 3].

In addition to these types of plasmonic oscillations, there are other resonances named plasmonic chain modes. These modes can be generated in linear arrays of

closely spaced metallic nanoparticles, including nanowires, and they result from the near field coupling between adjacent nanoparticles excited at their plasmonic resonances. Due to this coupling effect, light can propagate through the periodic arrays. Thus, these periodic structures can be regarded as discrete plasmonic waveguides [4–6]. When placing a periodic array of metallic nanoparticles in a layered media, under proper excitation conditions, the plasmonic chain modes can also couple to the SPP of a metallic substrate, forming hybrid SPP-chain modes [7].

In this same sense, when placing periodic arrays of metallic nanoparticles on top of dielectric waveguides, the plasmonic chain modes can couple to the photonic modes of the waveguide [8]. These integrated structures give rise to the so-called hybrid photonic-plasmonic waveguide modes [9], and they are the main subject of interest in this chapter. We will focus our attention to integrated structures consisting of periodic arrays of metallic nanowires integrated on top of two-dimensional dielectric photonic waveguides.

To this purpose, we will bring a comprehensive explanation about the physics behind the dispersion curves of integrated hybrid photonic-plasmonic waveguiding structures. Then will be studied the propagation of electromagnetic fields through the integrated systems varying the geometric cross-section of the metallic nanowires. For a better understanding, this comprehensive study will be accompanied by numerical simulations, making easier to elucidate the potential applications of these outstanding structures.

## 2. Hybrid photonic-plasmonic waveguides

### 2.1 Optical waveguides

From the analysis of the chemical composition of farer stars to imaging of microscopic living cells, information transport through light is one of the main subjects of interest in optical sciences. Among the different ways to transport light can be found optical waveguides, whose principle of operation is based on the total internal reflection effect. This phenomenon consists of the complete reflection of light within a medium surrounded by media with smaller refractive index, as depicted in **Figure 1**.

The schematic in **Figure 1a** represents an asymmetric planar waveguide invariant along the out-of-plane direction, consisting of a dielectric medium of refractive index  $n_2$  between two media of refractive index  $n_1$  and  $n_3$ , where  $n_2 > n_1 > n_3$ . As light propagates in the inner medium  $n_2$ , certain rays will present a phase difference of zero or a multiple of  $2\pi$ , when they are twice reflected. This situation means that

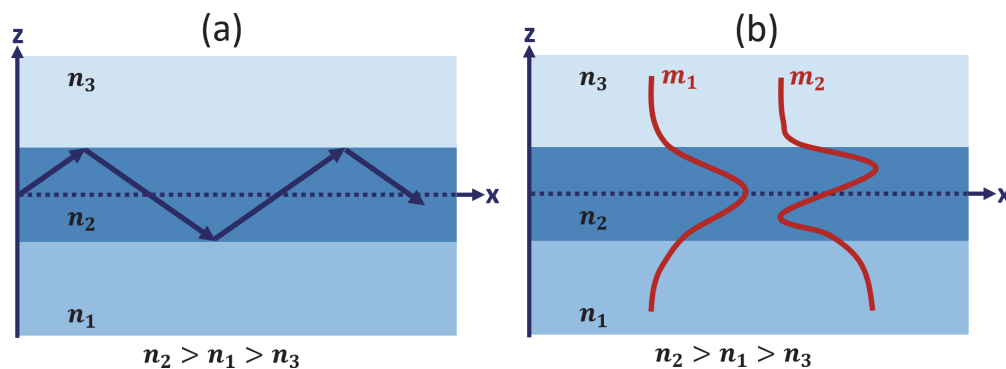


**Figure 1.** Schematic representation of a planar asymmetric waveguide consisting of three dielectric media of refractive index  $n_1$ ,  $n_2$  and  $n_3$ . (a) Self-consistency condition defining the modes of the waveguide. (b) Profile of the field distributions of the first two guided modes of the waveguide.

after a round-trip the wave reproduces itself, preserving the same spatial distribution and polarization along the waveguide. Fields satisfying this self-consistency condition are known as eigenmodes or modes of the waveguide [10]. The schematic in **Figure 1b** shows the profile of the field distribution for the first two modes of the proposed waveguide.

## 2.2 Dispersion relation

To determine the propagation constant of the modes supported by the waveguide, let us consider a waveguide with a core of refractive index  $n_2$  and thickness  $d$ , surrounded by two semi-infinite dielectric media of refractive index  $n_1$  and  $n_3$ , as depicted in **Figure 2**.

For each medium, the field can be represented as a sum of propagative and counter-propagative waves along the  $z$  axis, and propagative in the  $x$  direction that can be represented as

$$\psi_m(x, z, \omega) = A_m e^{-i\alpha_m z} e^{-i\beta_m x} e^{-i\omega t} + B_m e^{i\alpha_m z} e^{-i\beta_m x} e^{-i\omega t}, \quad (1)$$

where  $m = I, II, III$ ,  $A_m$  and  $B_m$  are the amplitudes of the propagative and counter-propagative waves, respectively, and the propagation constants  $\alpha_m$  and  $\beta_m$  along the  $z$  and  $x$  axis are related through

$$\beta_m = \sqrt{\left(\frac{\omega}{c}\right)^2 \varepsilon_m(\omega) - \alpha_m^2}, \quad (2)$$

where  $\varepsilon_m(\omega)$  is the dielectric constant of the  $m$ -th medium related to the refractive index by  $n_m = \sqrt{\varepsilon(\omega)\mu(\omega)}$ . At optical wavelengths, the magnetic permeability  $\mu(\omega)$  can be considered as unit. Eq. (2) is obtained from the Helmholtz and Maxwell equations [11].

At the interfaces  $z = 0$  and  $z = d$ , the electromagnetic field should be continuous, that is to say:

$$\psi_I(x, z, \omega)|_{z=0} = \psi_{II}(x, z, \omega)|_{z=0}, \quad (3)$$

and

$$\psi_{II}(x, z, \omega)|_{z=d} = \psi_{III}(x, z, \omega)|_{z=d}. \quad (4)$$

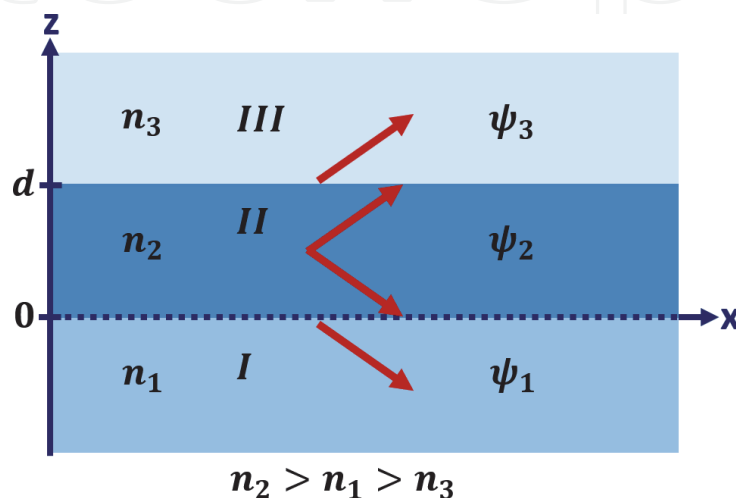


**Figure 2.**  
 Schematic representation of the field components in an asymmetric planar waveguide.

From the conservation of the tangential components of the electromagnetic field at the boundaries between two media [12] are obtained the relationships

$$\frac{1}{\nu_I} \frac{\partial \psi_I(x, z, \omega)}{\partial z} \Big|_{z=0} = \frac{1}{\nu_{II}} \frac{\partial \psi_{II}(x, z, \omega)}{\partial z} \Big|_{z=0}, \quad (5)$$

$$\frac{1}{\nu_{II}} \frac{\partial \psi_{II}(x, z, \omega)}{\partial z} \Big|_{z=-d} = \frac{1}{\nu_{III}} \frac{\partial \psi_{III}(x, z, \omega)}{\partial z} \Big|_{z=d}, \quad (6)$$

with  $\nu_m = 1$  for TE polarized electromagnetic fields and  $\nu_m = \varepsilon_m(\omega)$  for TM polarized fields. Substituting Eq. (1) in Eqs. (3–6), and considering that  $A_I = B_{III} = 0$  because both, *I* and *III* are semi-infinite media and no back-reflections from the boundaries are present, it is obtained a two coupled equation system that can be represented in a matrix way of the form

$$\begin{bmatrix} \frac{\alpha_I}{\nu_I} - \frac{\alpha_{II}}{\nu_{II}} & \frac{\alpha_I}{\nu_I} + \frac{\alpha_{II}}{\nu_{II}} \\ e^{-i\alpha_{II}d} \left( \frac{\alpha_I}{\nu_I} + \frac{\alpha_{III}}{\nu_{III}} \right) & -e^{-i\alpha_{II}d} \left( \frac{\alpha_I}{\nu_I} - \frac{\alpha_{III}}{\nu_{III}} \right) \end{bmatrix} \begin{bmatrix} A_{II} \\ B_{II} \end{bmatrix} = \begin{bmatrix} 0 \\ 0 \end{bmatrix}. \quad (7)$$

By equating to zero the determinant of the matrix it is possible to obtain the non-trivial solutions of this eigenmode equation system, resulting in the dispersion relation of a three-layered media

$$\frac{\left( \frac{\alpha_{II}}{\nu_{II}} - \frac{\alpha_I}{\nu_I} \right) \left( \frac{\alpha_{II}}{\nu_{II}} - \frac{\alpha_{III}}{\nu_{III}} \right)}{\left( \frac{\alpha_{II}}{\nu_{II}} + \frac{\alpha_I}{\nu_I} \right) \left( \frac{\alpha_{II}}{\nu_{II}} + \frac{\alpha_{III}}{\nu_{III}} \right)} = e^{i2d\alpha_{II}}. \quad (8)$$

We must notice that Eq. (8) is a transcendental function with no analytical solution, thus, numerical methods should be employed to solve it.

When solving this dispersion relation, it is obtained the mode propagation constant,  $\beta$ , that depends on the optical frequency or wavelength of light and determines how the amplitude and phase of light varies along the *x* direction. In the same way as wavenumber can be related to the refractive index of a homogeneous medium, the propagation constant can be regarded as the wavenumber (spatial frequency) of light propagating through an effective medium composed by the inhomogeneous three-layered structure. The propagation constant is then related to the so-called effective index through the relationship

$$\beta = \frac{2\pi}{\lambda} n_{eff}, \quad (9)$$

being  $\lambda$  the wavelength of light in vacuum. We must notice that the effective index is only defined for a mode of the waveguide and it should not be understood as a material property. We can say then that each mode of the waveguide will “see” different effective media.

As the refractive index of a dielectric medium, as well as the dielectric constant, is a real number equal or greater than the unit ( $n \geq 1$ ) the modes in a dielectric waveguide are diffraction limited: if the thickness of the waveguide,  $d$ , is smaller than  $\lambda/(2n_{eff})$ , the solutions for the dispersion Eq. (8) will lead to evanescent waves, meaning that no modes can be propagated below this limit.



## 2.3 Plasmonic waveguides

As previously explained, dielectric waveguides guide light modes by using the total internal reflection principle and self-consistency condition. These waveguides are diffraction limited due to the dielectric constant values. However, if the dielectric constant is a complex number, it would be possible to obtain solutions to the dispersion relation (Eq. 8) below the diffraction limit. This is the case of metallic materials. Hence, if at least one of the three media in the waveguide structure is metallic, it is always possible to obtain a propagative mode in the structure. The price to pay for this solution is that due to ohmic losses in metals, these modes propagate just few microns, in opposition to dielectric waveguides where light can propagate through kilometers.

These structures are known as plasmonic waveguides, and their operation principle is based on SPP mode propagation. These surface waves are the result of collective oscillations of the conductive electrons at a metal-dielectric interface induced by the electric field of an electromagnetic wave. For a system invariant in the  $\hat{y}$  direction, SPP modes can only be excited if the electric field oscillates in the  $xz$  plane. Hence, only TM polarized electromagnetic fields couple to SPP modes (for TE polarized waves the electric field only oscillates along the  $\hat{y}$  direction).

Different combinations of insulator (I) and metallic (M) materials can be used to define a plasmonic waveguide. In **Figure 3** are represented IIM, IMI and MIM plasmonic waveguide structures as well as the amplitude distribution of the out-of-plane electromagnetic field ( $H_y$  component) of the SPP modes. For the IIM structure, there is only one SPP mode at the interface between the metal ( $\epsilon_m$ ) and first dielectric ( $\epsilon_{d1}$ ). For both IMI and MIM configurations, two SPP modes can be excited. They result from in-phase and out-of-phase coupling of SPP at the first and second dielectric-metal interfaces, and they are known as symmetric and antisymmetric modes, respectively.

As plasmonic waveguides allow light propagation beyond the diffraction limit, these structures have been used for the development of integrated nanophotonic devices for optical signal transportation, optical communications, biosensing and even imaging applications [13–15].

## 2.4 Hybrid photonic-plasmonic waveguides

From the previous waveguiding configurations, it is natural to think that modes propagating through a dielectric waveguide can be coupled to a plasmonic waveguide. This kind of structures is named hybrid photonic-plasmonic waveguide, or simply hybrid plasmonic waveguide.

The structure depicted in **Figure 3a** can be considered as a hybrid plasmonic waveguide, but more complex multilayered systems can be designed to propagate more than one mode in these structures. For instance, in **Figure 4** are presented two

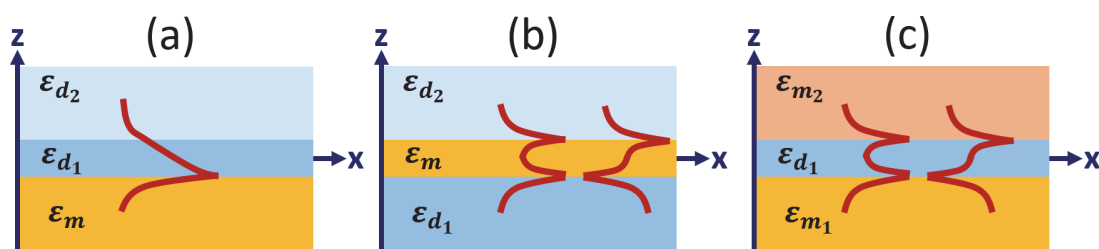


**Figure 3.** Schematic representation of plasmonic waveguides for (a) IIM, (b) IMI and (c) MIM configurations and SPP modes profiles. For IMI and MIM waveguides, symmetric and antisymmetric modes are excited.

examples of hybrid plasmonic waveguides able to support symmetric and antisymmetric SPP modes coupled to photonic modes of a dielectric waveguide.

To compute the supported modes of these structures, we can make use of the dispersion relation for a N-layered medium in terms of the T-matrix that relates the amplitudes of propagative and counter-propagative waves,  $A_m$  and  $B_m$ , in the  $m$ -th medium, to those from the  $m + 1$  medium through the relationship [16].

$$\begin{bmatrix} A_{N+1} \\ B_{N+1} \end{bmatrix} = [\mathbb{T}] \begin{bmatrix} A_1 \\ B_1 \end{bmatrix} = \prod_{m=1}^N [T_m] \begin{bmatrix} A_1 \\ B_1 \end{bmatrix} = \begin{bmatrix} t_{11} & t_{12} \\ t_{21} & t_{22} \end{bmatrix} \begin{bmatrix} A_1 \\ B_1 \end{bmatrix}, \quad (10)$$

where  $A_1 = B_{N+1} = 0$  (no back reflections from substrate and superstrate) and

$$[T_m] = \frac{1}{2} \begin{bmatrix} (1 + \gamma)e^{-i(k_m - k_{m+1})} & (1 - \gamma)e^{i(k_m + k_{m+1})} \\ (1 - \gamma)e^{-i(k_m + k_{m+1})} & (1 + \gamma)e^{i(k_m - k_{m+1})} \end{bmatrix}, \quad (11)$$

with  $k_m = \alpha_m d_m$ ,  $k_{m+1} = \alpha_{m+1} d_{m+1}$ ,  $\gamma = (\alpha_m \nu_{m+1}) / (\alpha_{m+1} \nu_m)$ , being  $d_j$  the position of the interface between  $j$  and  $j + 1$  media, considering that  $d_{N+1} = d_N$  and  $\nu_m = 1$  for TE polarized electromagnetic fields and  $\nu_m = \epsilon_m(\omega)$  for TM polarized fields. By equating to zero the term  $t_{22}$  of the  $\mathbb{T}$  matrix, we can directly obtain the propagation constant of the modes supported by the structure.

## 2.5 Dispersion curves and mode analysis

Before studying light propagation in complex hybrid plasmonic waveguides, it is worthily to briefly comment on the dispersion diagrams that would help to perform an analysis of the modes propagating through these waveguides. So far, we have presented the dispersion relation for a multilayered media. It is not our intention to explore the numerical methods that can be employed to solve this transcendental equation, but to analyze the information obtained from these results. The reader can look at references [17–22] to have an insight of how to solve the dispersion relation.

As an example, let us analyze the modes of a four-layered media as schematized in **Figure 4a**, consisting of a glass substrate with refractive index  $n_1 = 1.5$ , a silicon nitride layer (core of the photonic waveguide) of thickness  $d = 300$  nm and refractive index  $n_c = 2.0$ , a thin gold layer of thickness  $t = 40$  nm, and air superstrate ( $n_2 = 1.0$ ). The numerical results obtained from the calculation of the dispersion relation for TM polarized fields by using the Raphson–Newton method [23] are plotted in **Figure 5**. For these calculations was considered a spectral wavelength range from 400 nm to 1  $\mu$ m, and effective index range between 0.9 and 2.5. Since

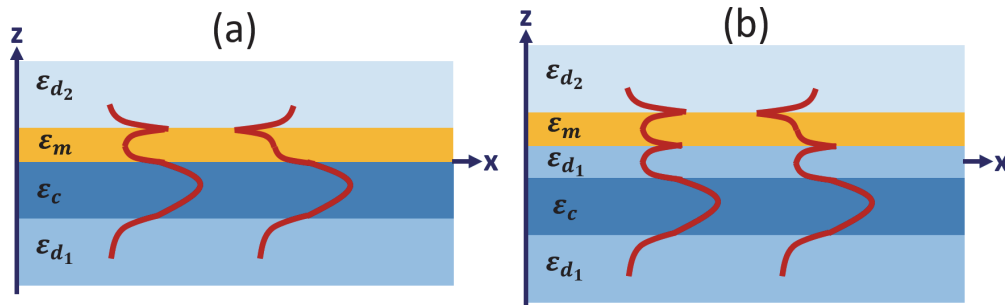


**Figure 4.** Schematic representation of hybrid photonic-plasmonic waveguides and mode profiles for (a) a metallic layer placed directly on top of the dielectric waveguide, and (b) with an intermediate dielectric layer between photonic and plasmonic waveguides. In both systems, the fundamental mode of the waveguide couple to the symmetric and antisymmetric SPP modes.

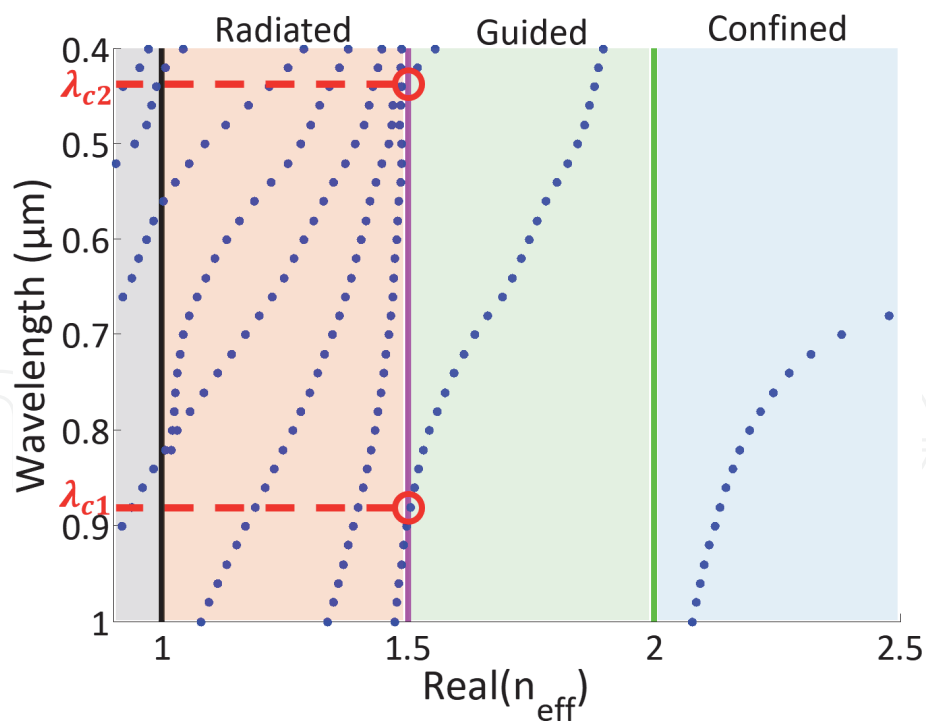


**Figure 5.**  
 Dispersion curves for a hybrid photonic-plasmonic waveguide consisting of a glass substrate ( $n_1 = 1.5$ ), silicon nitride core of 300 nm thickness ( $n_c = 2.0$ ), a thin gold layer of thickness 40 nm, and an air superstrate ( $n_2 = 1.0$ ). The numerical results show a confined mode (blue region) and two guided modes (green region). At the orange region, many radiated modes were obtained, as well as many non-physical solutions (gray region).

the results are just numerical solutions, we need to understand the physical meaning for each solution.

The vertical constant lines at 1, 1.5 and 2.0 correspond to the refractive index of each dielectric medium: air superstrate, glass substrate and silicon nitride core, respectively. These vertical lines are also referred as light lines, as they are linked to the propagation constant of light traveling in that specific homogeneous medium through Eq. (9).

These light lines define four different regions. The first region, for effective index values below 1 (gray region), are numerical solutions without physical meaning: if the effective index is smaller than unit, the modes would travel faster than speed of light in vacuum (which obviously is not our case). The second region between the refractive index of glass and air refractive index (orange region) defines modes with effective index smaller than glass but greater than air. Hence, they are modes whose energy is propagating in the glass substrate, and they are referred as radiated modes. The third region, between the silicon nitride (core) light line and glass light line, define modes whose energy is propagating in the core of the waveguide: as the effective index is higher than glass substrate index, the energy of these modes does not propagates in glass, so the energy is confined in the core. These are guided modes. The value at which the effective index of these modes matches the refractive index of the glass substrate determines the cut-off wavelength of guided modes. For the analyzed example, these values are  $\lambda_{c1} = 886$  nm and  $\lambda_{c2} = 430$  nm (red circles).

The fourth region (blue colored) correspond to modes whose energy does not propagates in any of the dielectric layers: their effective index is greater than the core, substrate, and superstrate. Hence, these modes are confined to the metallic layer. These solutions correspond to propagative SPP modes and they are referred as confined modes.

In literature, different representations of the dispersion curves can be found, like propagation constant vs. frequency (usually normalized to a reference value),



wavelength vs. incidence angle (used in attenuated total internal reflection measurements), among others. The representation that we use in **Figure 5** allows us to understand the dispersion curves in terms of two quantities that can be easily identified: wavelength and effective index.

## 2.6 Mode hybridization

To further understand the origin of the modes appearing in the hybrid photonic-plasmonic structure, let us analyze the multilayered system by parts: first we will compute the dispersion curves of the photonic waveguide (**Figure 6a**), then the modes of the plasmonic waveguide (**Figure 6b**), and finally compare them with the full hybrid photonic-plasmonic structure (**Figure 6c**). The numerical results for the dispersion relation of each one of these cases are presented in **Figure 6d**. The dimensions of the structures are the same than those used for **Figure 5**.

The blue dots and circles in guided region, correspond to the fundamental  $TM_0$  and higher order  $TM_1$  modes of the silicon nitride waveguide (thickness  $d = 300$  nm and refractive index  $n_c = 2.0$ ) surrounded by air superstrate ( $n_{sup} = 1.0$ ) and glass substrate ( $n_{sub} = 1.5$ ), as depicted in **Figure 6a**. These modes present cut-off wavelength values around  $\lambda_{TM0} = 1.58 \mu\text{m}$  and  $\lambda_{TM1} = 545$  nm, respectively.

When computing the modes of a thin gold layer of thickness  $t = 40$  nm on top of a glass substrate ( $n_{sub} = 1.5$ ) and air superstrate, as depicted in **Figure 6b**, it is observed one mode in the guided region that tends to a constant value (red dots in **Figure 6d**). For this structure, we must notice that no core was present, then, the effective index of this mode is higher than the refractive index of the glass substrate, hence, it is a SPP mode confined to the metallic layer.

We can observe that both,  $TM_0$  and SPP modes, cross each other around an effective index value of 1.798. In other words, the propagation constant for both modes are the same, so they are phase matched. This situation means that the photonic mode of the waveguide will excite the plasmonic mode of the metallic layer.

When the modes of the complete integrated structure (**Figure 6c**) are computed, two branches are observed. The first one, represented by red triangles, is a

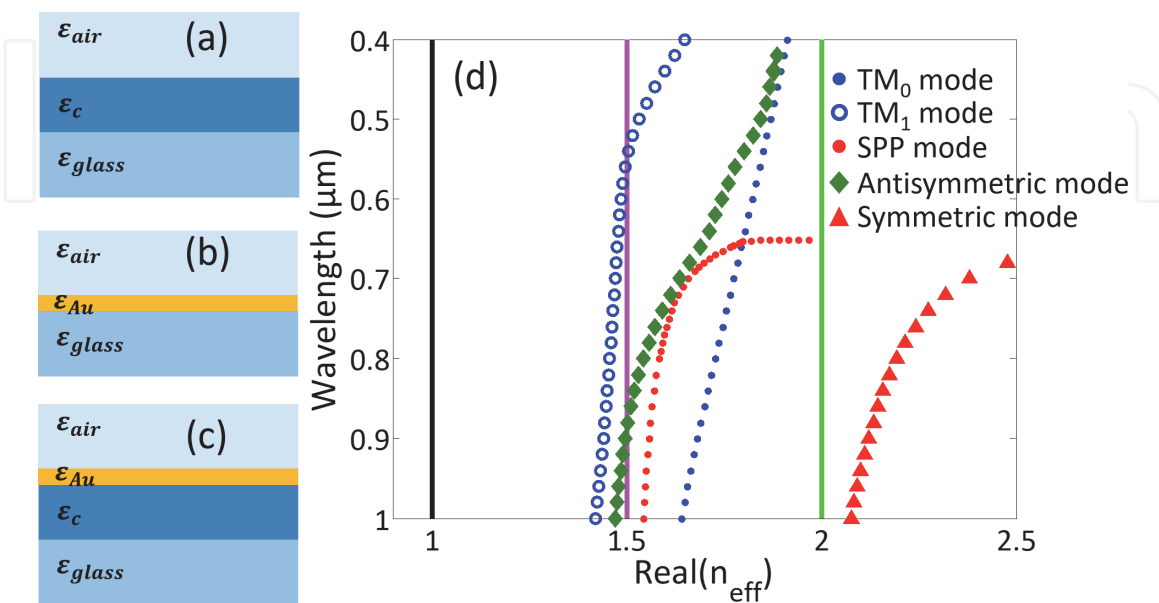


**Figure 6.** Schematic representation of (a) photonic waveguide, (b) plasmonic waveguide, and (c) hybrid photonic-plasmonic waveguide. (d) Dispersion curves for the three studied structures. Due to phase matching between  $TM_0$  and SPP modes, hybrid symmetric and antisymmetric modes arise in the full integrated structure.

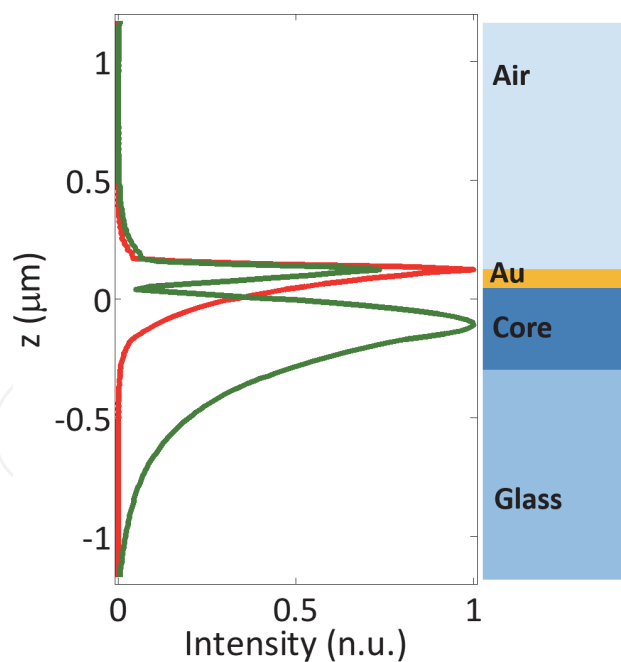


**Figure 7.** Intensity profiles of the symmetric (red) and antisymmetric (green) modes of the hybrid photonic plasmonic waveguide at  $\lambda = 750 \text{ nm}$ . The symmetric mode is mainly confined in the metallic layer, while the antisymmetric presents amplitude in both, photonic and plasmonic waveguides.

mode confined to the metallic layer, and the second one, relies in the guided region (green diamonds). These modes arise from the coupling of the  $TM_0$  and SPP modes, and they are referred as hybrid modes, being the first one a symmetric mode and the second an antisymmetric mode.

It is important to say that both symmetric and antisymmetric modes are not independent, they are hybrid modes. Like in two coupled harmonic oscillators, this hybridization means that there is an energy exchange between photonic and plasmonic waveguides. For the symmetric mode, the amplitude of light in both, photonic and plasmonic waveguides, are in phase, while for the antisymmetric are out-of-phase [24, 25].

Finally, in **Figure 7** are plotted the normalized intensity profiles of the symmetric (red curve) and antisymmetric (green curve) modes at a wavelength of  $\lambda = 750 \text{ nm}$ . The intensity is derived from the amplitudes of Eq. 1. As expected from the dispersion curves, the intensity of the symmetric mode is mainly confined in the metallic layer (the mode solution relies in the confined region), while for the antisymmetric mode the intensity is distributed in both photonic and plasmonic waveguides, being greater the intensity in the dielectric region (the solution relies in the guided region).

### 3. Mode propagation in a periodic array of metallic nanowires

In general, plasmonic resonances in metallic nanostructures are divided in two kinds, namely SPP and LSP. SPP modes are propagative waves confined at the dielectric/metal interface, while LSP are standing waves or cavity modes oscillating in a nanoparticle.

As it is well known, LSP resonances depend not only on the material of the nanoparticles, but also on their shape and polarization of the incident wave: the orientation of the electric field defines the direction of the oscillation of the charges in the metallic nanoparticle; these charges will distribute depending on the geometry of the particle, giving rise to different modes. For small nanoparticles, usually

are only excited dipolar LSP resonances, but quadrupoles, octupoles and higher order modes can also be excited.

When metallic nanoparticles are closely placed and excited at their LSP resonance, it is possible to couple them via near field interaction, leading to higher order LSP modes. To understand this coupling mechanism, let us take a look to **Figure 8**, where a dimer of spherical metallic nanoparticles oriented along the  $x$  axis (dimer axis), is excited with electric field oscillating in  $z$  and  $x$  directions.

When the electric field is oriented along the  $z$  axis, perpendicular to the dimer axis, the dipolar resonances of the nanoparticles are oriented also in the  $z$  direction. If the dipoles are in phase (**Figure 8a**), the dimer also presents a dipolar resonance. If the dipoles are out-of-phase (**Figure 8b**), the dimer presents a quadrupolar resonance. Since the distribution of the charges is perpendicular to the dimer axis, both modes are referred as dipolar and quadrupolar transverse modes, respectively.

If the electric field oscillates along the  $x$  axis, the dipoles of the nanoparticles will be oriented along the dimer axis, thus, the coupled modes are called dipolar longitudinal modes. If the dipoles are in phase (**Figure 8c**), the resonance wavelength of the longitudinal mode will be shorter than the resonance wavelength of the out-of-phase dipoles (**Figure 8d**).

In the same way, a periodic array of metallic nanoparticles can be coupled, allowing light propagation. Thus, when properly excited, a periodic array of metallic nanoparticles can be regarded as a plasmonic waveguide. These resonances are named plasmonic chain modes, and their waveguiding properties will depend on the shape and period of the nanoparticles, as well as the orientation of the incident electromagnetic field. Besides energy transportation capabilities, these modes have been widely studied because they allow a strong enhancement of the electromagnetic field in a localized nanometric region.

If we consider that the nanoparticles in **Figure 8** are invariant in the out-of-plane  $y$  direction, the same coupling mechanism is preserved. These structures are named metallic nanowires (MNW): metallic nanostructures with nanometric cross section and micrometric lengths. As the length of the nanowires is times longer than the incident wavelength, the absorption of light prevents from the formation of cavity modes in this direction. This means that plasmonic resonances in metallic nanowires can be excited only if the electric field is perpendicular to the invariant

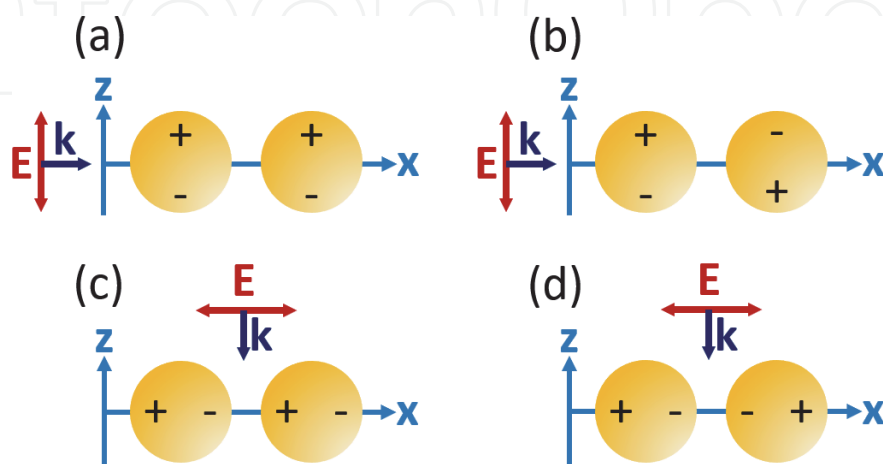


**Figure 8.** LSP coupled modes for spherical nanoparticle dimers. When the electric field is perpendicular to the main axis of the dimer are excited (a) dipolar and (b) quadrupolar transverse modes. When the electric field is parallel to the main axis of the dimer, dipolar longitudinal modes of (c) shorter and (d) longer resonant wavelengths are obtained.

$y$  axis, i. e. with TM polarized light. Thus, the plasmonic chain modes in metallic nanowires will mainly depend on the geometry of their cross section [26–28].

### 3.1 Plasmonic chain modes in MNW with rectangular cross section

Let us consider an infinite periodic array of gold nanowires of width  $w = 80$  nm, gap between them  $g = 50$  nm (period  $\Lambda = 130$  nm) and thickness  $t = 20$  nm, embedded in a homogeneous dielectric medium of refractive index  $n_d = 1.5$  (glass), as depicted in **Figure 9a**. The structure is invariant along the out-of-plane direction.

To perform a modal analysis, it is required to compute the dispersion curves of these system. Different numerical methods can be employed, like effective index method [29–31], source model technique [32], rigorous coupled wave analysis (RCWA) [33–35], or Fourier modal method (FMM) [36–39], among others.

In our case, we will make use of the FMM to compute the dispersion curves of the periodic structure. This rigorous method computes the Maxwell equations in the frequency domain. To solve them, a unit cell of the periodic structure, as well as the dielectric function and electromagnetic field are expanded in Fourier series. This formulation leads to an eigenvalue matrix formulation that can be used to obtain the modes of the nanowires in a multilayered media. Also, by adding perfectly matched layers (PML), it is possible to compute the beam propagation in a finite periodic structure. It is not our intention to show how to implement this numerical method, but to analyze plasmonic chain modes in periodic MNW. For a better comprehension about this method, we invite the reader to look at references [37, 38].

The plot in **Figure 9b** corresponds to the dispersion curves of the system under study. As we are dealing with a periodic structure, it is useful to represent this plot in terms of the propagation constant (along the periodicity direction), normalized to the Bragg condition ( $\beta = \pi/\Lambda$ ), which defines the first Brillouin zone (vertical black line). The red dotted curve represents the modes supported by the MNW, as they are confined below the glass light-line. To understand the behavior of this

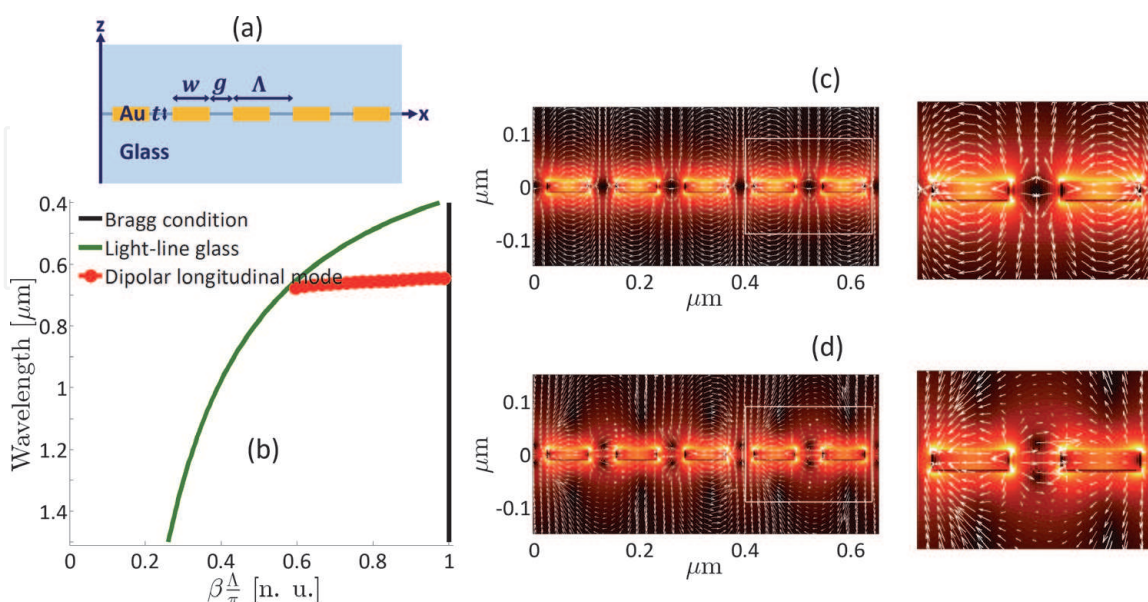


**Figure 9.** (a) Schematic representation of a periodic infinite array of gold nanowires of width  $w = 80$  nm, gap  $g = 50$  nm, period  $\Lambda = 130$  nm and thickness  $t = 20$  nm in a homogeneous dielectric medium. (b) the confined modes below the glass light-line (green curve) correspond to a dipolar longitudinal mode (red dotted curve). (c) the energy density map and electric field lines computed at the Bragg condition ( $\lambda = 645$  nm), reveals the dipolar longitudinal coupling between MNW. (d) out of the Bragg condition, at  $\lambda = 667$  nm, we still observe the dipolar coupling.



plasmonic mode, it is necessary to observe the distribution of the charges in the MNW.

In **Figure 9c** are shown the energy density map and electric field lines distribution of the plasmonic mode at  $\lambda = 645$  nm. At this wavelength, the red curve crosses the Bragg condition, defining a stationary mode. As we can observe, MNW are coupled, with a phase shift of  $\pi$  rad between them. Thus, it is a plasmonic chain mode. Out of the Bragg condition, for instance, at  $\lambda = 667$  nm ( $\beta = 0.641\pi/\Lambda$ ), the chain mode becomes propagative and the electric field lines remain almost longitudinally oriented inside the MNW (**Figure 9d**). In view of the phase shift and the orientation of the electric field lines, the plasmonic chain mode results from coupled dipolar resonances oriented along the  $x$  axis. Thus, the red dotted curve corresponds to the dispersion relation of a dipolar longitudinal plasmonic chain mode.

As defined for a SPP, the propagation length of this plasmonic chain mode can be computed through the relationship

$$L_p = \frac{1}{2\beta''}, \quad (12)$$

where  $\beta''$  is the imaginary part of the propagation constant. In our structure, the propagation length varies from  $L_p = 200$  nm (for wavevectors close to the glass light-line) up to  $L_p = 1.14$   $\mu$ m (for wavevectors near the Bragg condition).

### 3.2 Hybrid plasmonic chain modes in MNW integrated to a dielectric waveguide

Now, let us study a hybrid photonic-plasmonic system consisting of a dielectric waveguide of thickness  $d = 200$  and refractive index  $n_{wg} = 2.0$ , on top of which is placed, at a distance  $h = 30$  nm, a periodic array of gold nanowires with the same parameters than those of the previous subsection, as depicted in **Figure 10a**.

The dispersion curves in the first Brillouin zone, obtained with the FMM, are shown in **Figure 10b**. The green and magenta curves represent the glass and waveguide light lines, respectively, while the black vertical line represents the Bragg condition. The blue triangles curve corresponds to the fundamental  $TM_0$  photonic guided mode without the presence of the MNW, while the green asterisk curve is the dispersion curve of the dipolar longitudinal plasmonic chain mode (without the presence of the waveguide). As can be observed, there is an intersection point between the  $TM_0$  and dipolar longitudinal modes in the guided region around a wavelength value  $\lambda = 664$  nm (**Figure 10c**). This crossing point means that both modes have the same propagation constant ( $\beta = 0.672(\pi/\Lambda)$ ), hence, they will couple when placing them near to each other, leading to a hybrid photonic-plasmonic mode. As a result, symmetric and anti-symmetric modes will arise. This hybridization is corroborated when computing the dispersion curves of the integrated system, being observed two curves: a lower branch passing from guided to confined region (red circles) and an upper branch in the guided region. In analogy with a two coupled waveguide system, this situation means that, for the lower branch, energy from the  $TM_0$  mode is converted into plasmonic chain mode; for the upper branch, the energy from the plasmonic chain mode is converted into  $TM_0$  mode. This anti-crossing phenomenon is the characteristic signature of strong coupling between guided modes.

To corroborate the symmetry of these modes, in **Figure 11** we plot the energy density maps and electric field lines distribution for both modes at the Bragg condition. **Figure 11a** corresponds to the energy density map computed for the upper branch at  $\lambda = 473$  nm, where we can observe that the energy is distributed in



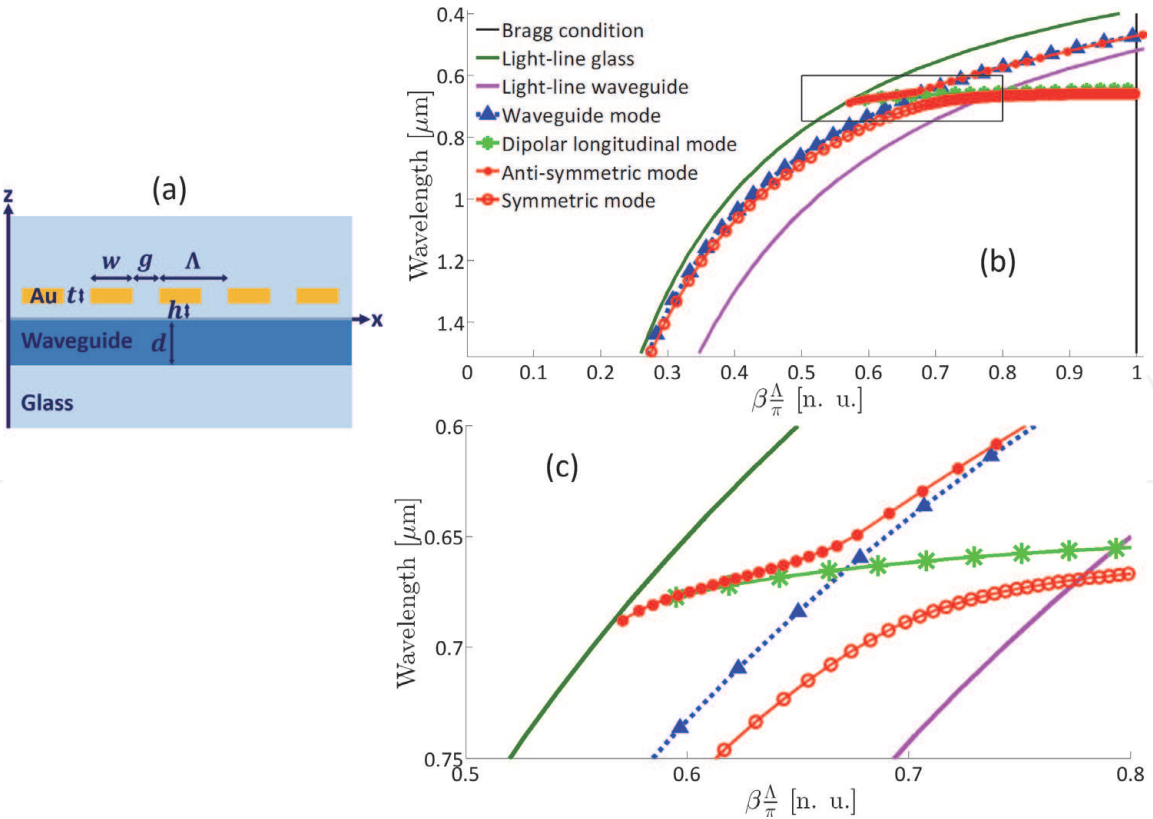


**Figure 10.** (a) Schematic representation of the integrated structure consisting of an infinite periodic arrays of gold nanowires ( $w = 80\text{ nm}$ ,  $g = 50\text{ nm}$ ,  $\Lambda = 130\text{ nm}$ ,  $t = 20\text{ nm}$ ) surrounded by glass ( $n_s = 1.5$ ), placed on top of a dielectric waveguide ( $d = 200\text{ nm}$ ,  $n_{wg} = 2.0$ ) at a distance  $h = 30\text{ nm}$ . (b) Dispersion curves of the integrated system. (c) Inset at the anti-crossing region.

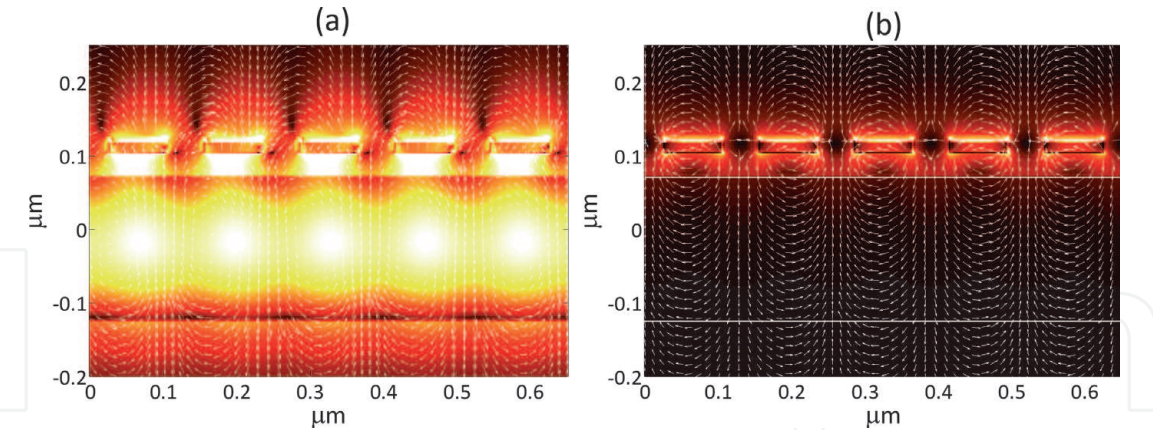


**Figure 11.** Energy density maps and electric field lines distribution for (a) the antisymmetric mode at  $\lambda = 473\text{ nm}$ , and (b) for the symmetric mode at  $\lambda = 660\text{ nm}$ .

the dielectric waveguide and the periodic array of MNW. When looking at the electric field lines, it is observed a phase difference between these vectors above and below the MNW, defining an antisymmetric quadrupolar chain mode. For the case of the lower branch, computed at  $\lambda = 660\text{ nm}$  (**Figure 11b**), the energy is confined to the MNW and not in the waveguide, as expected from the dispersion curves. For this case, the electric field lines above and below the MNW are in phase, defining a symmetric dipolar chain mode.

Finally, by making use of the aperiodic Fourier modal method [27, 39], and considering a finite number of 27 MNW, we computed the transmission

(red curve), reflection (blue dashed curve), and absorption (black dotted curve) spectra of light propagating through the integrated system, normalized to the incident beam (**Figure 12a**). The reflection spectrum (blue dashed curve) exhibits a maximum peak around  $\lambda = 474$  nm, while the transmission spectrum shows a broad depth around  $\lambda = 520$  nm and a narrower depth around  $\lambda = 678$  nm. The first depth (close to the maximum in reflection) is due to a Bragg reflection induced by the periodic array of MNW. This condition can be verified with the expression

$$\lambda_{\text{Bragg}} = \frac{2n_{\text{eff}}\Lambda}{m}, \quad (13)$$

where  $n_{\text{eff}}$  is the effective index of the mode,  $\Lambda$  the period of the MNW array, and  $m$  the Bragg order. According to the dispersion curves, at  $\lambda = 520$  nm, the effective index of the antisymmetric mode is  $n_{\text{eff}} = 1.801$ , and considering the period  $\Lambda = 130$  nm, the first order Bragg reflection will occur at  $\lambda_{\text{Bragg}} = 468$  nm, which is a value close to the maximum in the reflection spectrum. The near field map in **Figure 12b**, shows the amplitude of the  $H_y$  field component, where are observed periodic lobes inside the waveguide core due to the Bragg reflection.

The second depth on the transmission spectrum corresponds to the excitation of the dipolar longitudinal plasmonic chain mode. In the dispersion curves, this wavelength value corresponds to the anti-crossing point between symmetric and antisymmetric modes, around  $\beta = 0.672(\pi/\Lambda)$ . As expected, at this wavelength the plasmonic chain mode is efficiently coupled to the photonic  $TM_0$  mode of the waveguide, leading to an energy exchange between the photonic waveguide and the periodic array of MNW, as illustrated in the near field map of **Figure 12c**.

### 3.3 Hybrid plasmonic chain modes in MNW of triangular cross section integrated to a dielectric waveguide

Among the large variety of shapes in nanowires, sharp geometries such as nanotips stimulate a great interest in applications where a strong localization of the electromagnetic field is required. These triangular geometries present an

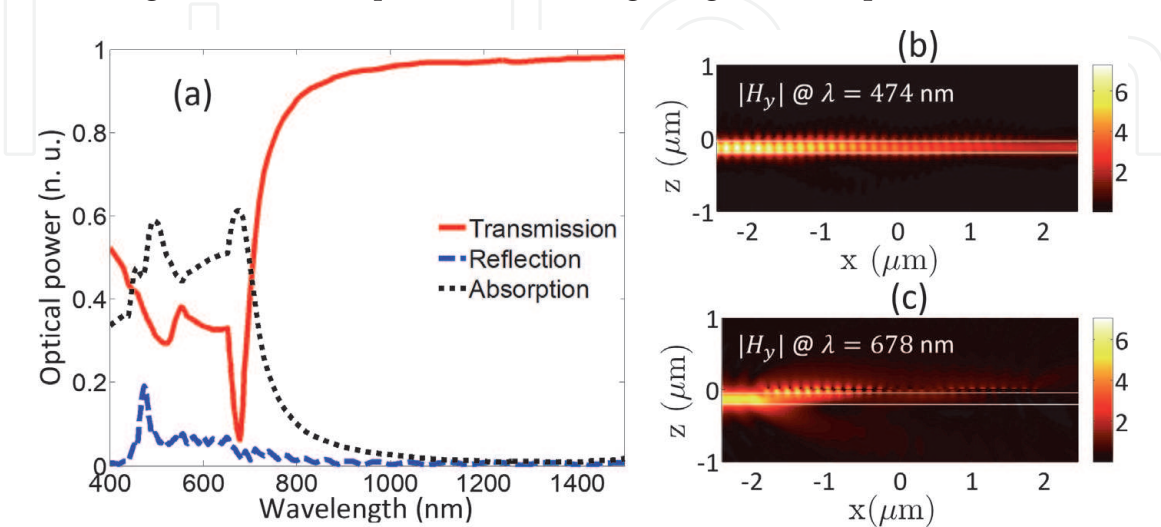


**Figure 12.** (a) Normalized transmission (red), reflection (blue dashed) and absorption (black dotted) spectra of light propagating through the waveguide in the integrated device. (b) At  $\lambda = 474$  nm, the  $H_y$  field component exhibits a Bragg reflection, while at (c)  $\lambda = 678$  nm, it is observed an energy exchange between the waveguide and periodic array of MNW.

extraordinary enhancement of light in the vicinity of their apex resulting from the excitation of LSP resonances polarized along their tip axis. In this section, we will study the excitation of plasmonic chain modes in periodic arrays of gold nanowires with triangular cross section through the photonic mode of a dielectric waveguide.

Firstly, we will study the plasmonic chain modes of the MNW placed on top of a glass substrate and the photonic modes of the dielectric waveguide that will be used to excite them. The MNW consist of an infinite periodic array of gold nanowires with triangular cross section of height  $t = 144$  nm, width  $w = 72$  nm, and period  $\Lambda = 200$  nm, placed on top of a glass substrate ( $n_{sub} = 1.5$ ). The superstrate is air ( $n_{sup} = 1.0$ ), the tip radius of the nanowires is  $r = 5$  nm, and the system is invariant in the out-of-plane  $y$  direction, as depicted in **Figure 13a**. Then dielectric waveguide consist of a core of thickness  $d = 200$  nm and refractive index  $n_{wg} = 2.0$ , buried a distance  $h = 30$  nm from the glass/air interface (**Figure 13b**).

The dispersion curves in the first Brillouin zone are plotted in **Figure 13c**, where can be observed the light lines of air superstrate (white curve), glass substrate (black curve) and core of the waveguide (green curve). The colored regions correspond to the normalized absorption spectra obtained when illuminating the structure from the substrate with a plane wave and mapped into  $\beta = k_0 n_{sub} \sin \theta_{inc} \Lambda / \pi$  (see reference [28] for a detailed explanation). The blue triangles curve in the guided region correspond to the fundamental  $TM_0$  photonic mode of the isolated waveguide. The array of MNW supports plasmonic chain modes. The first one is a

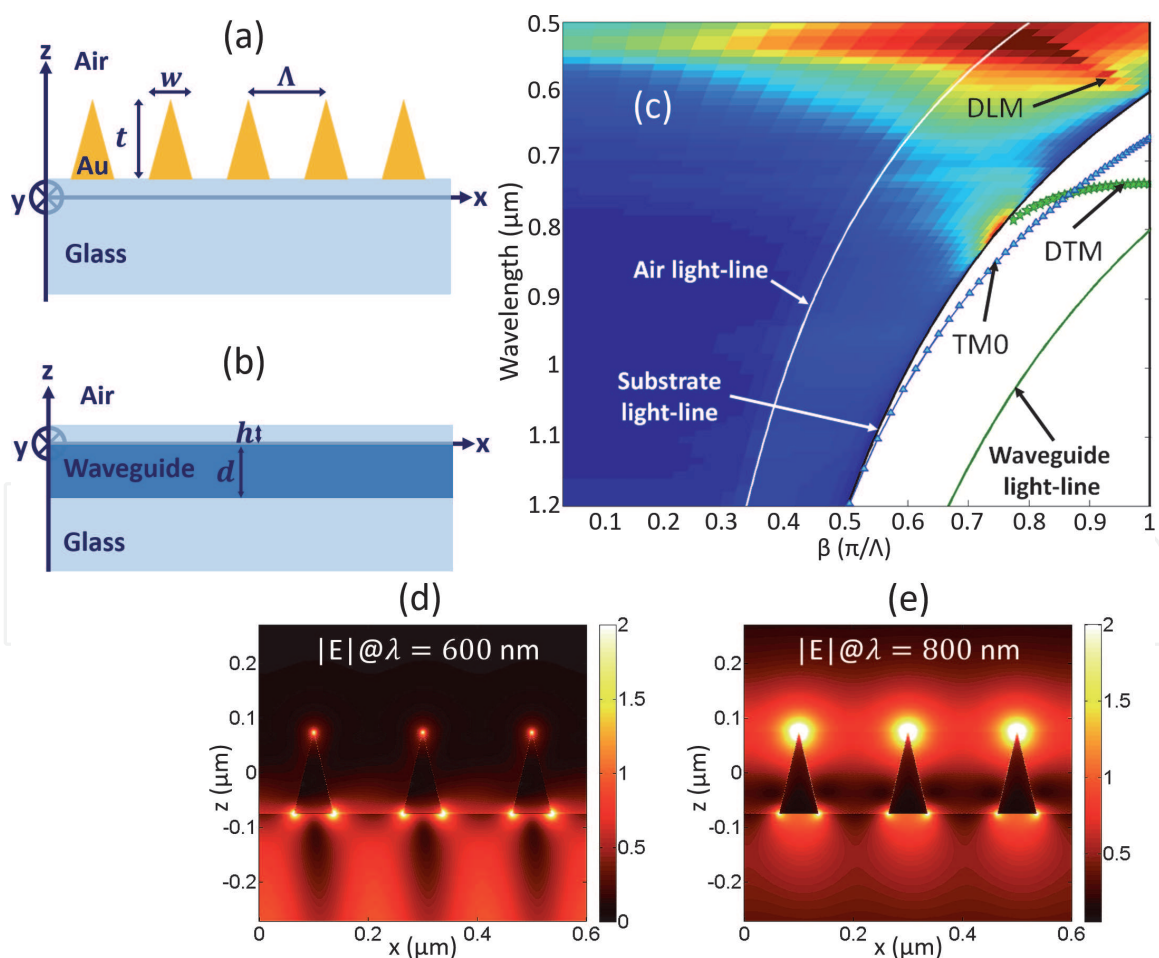


**Figure 13.** Schematic representation of (a) periodic array of gold nanowires with triangular cross section ( $w = 72$  nm,  $t = 144$  nm,  $\Lambda = 200$  nm) on top of a glass substrate surrounded by air, and (b) a dielectric waveguide of thickness  $d = 200$  nm and refractive index  $n_{wg} = 2.0$  buried a depth  $h_1 = 30$  nm in a glass substrate. (c) Dispersion curves of the  $TM_0$  mode supported by the waveguide (blue triangles), dipolar longitudinal mode (radiated to the substrate) and dipolar longitudinal mode (green stars). Energy density maps of (d) DLM at  $\lambda = 600$  nm and (e) DTM at  $\lambda = 800$  nm.



dipolar longitudinal mode (DLM) radiating into the substrate (which is barely excited at the Bragg condition). This mode is characterized by charges coupling and electromagnetic field enhancement at the base (bottom apexes) of the nanowires, as can be observed in the energy density map in **Figure 13d**. The second plasmonic chain mode (green stars) is a dipolar transverse mode (DTM) resulting from coupling of dipoles oriented along the  $z$  axis. This guided mode is characterized by a strong electromagnetic field enhancement at the upper apexes of the nanowires, as can be observed in **Figure 13e**. We can notice in the dispersion curves that at  $\lambda = 747$  nm ( $\beta = 0.86\pi/\Lambda$ ), the DTM crosses the  $TM_0$  mode of the waveguide, situation that will lead to a strong coupling between these modes when integrating both waveguiding systems.

When integrating the MNW on top of the dielectric waveguide (**Figure 14a**), the dispersion curves shows three modes in the guided region (**Figure 14b**), one corresponding to the DLM (magenta circles) and two other branches corresponding to the anti-symmetric (blue circles) and symmetric (red dots) dipolar transverse chain modes. The mode splitting between these two last resonances arises from strong coupling between dipolar transverse and  $TM_0$  modes. The near field maps in **Figure 14c** present the amplitude and phase of the  $H_y$  field for the DLM, where is observed a field enhancement below each nanowire and in the waveguide region. For the antisymmetric DTM (**Figure 14d**) the field is mainly enhanced in the waveguide region, with a phase difference of  $\pi$  rad between the MNW and the waveguide; for the symmetric DTM (**Figure 14e**), the field is enhanced between the

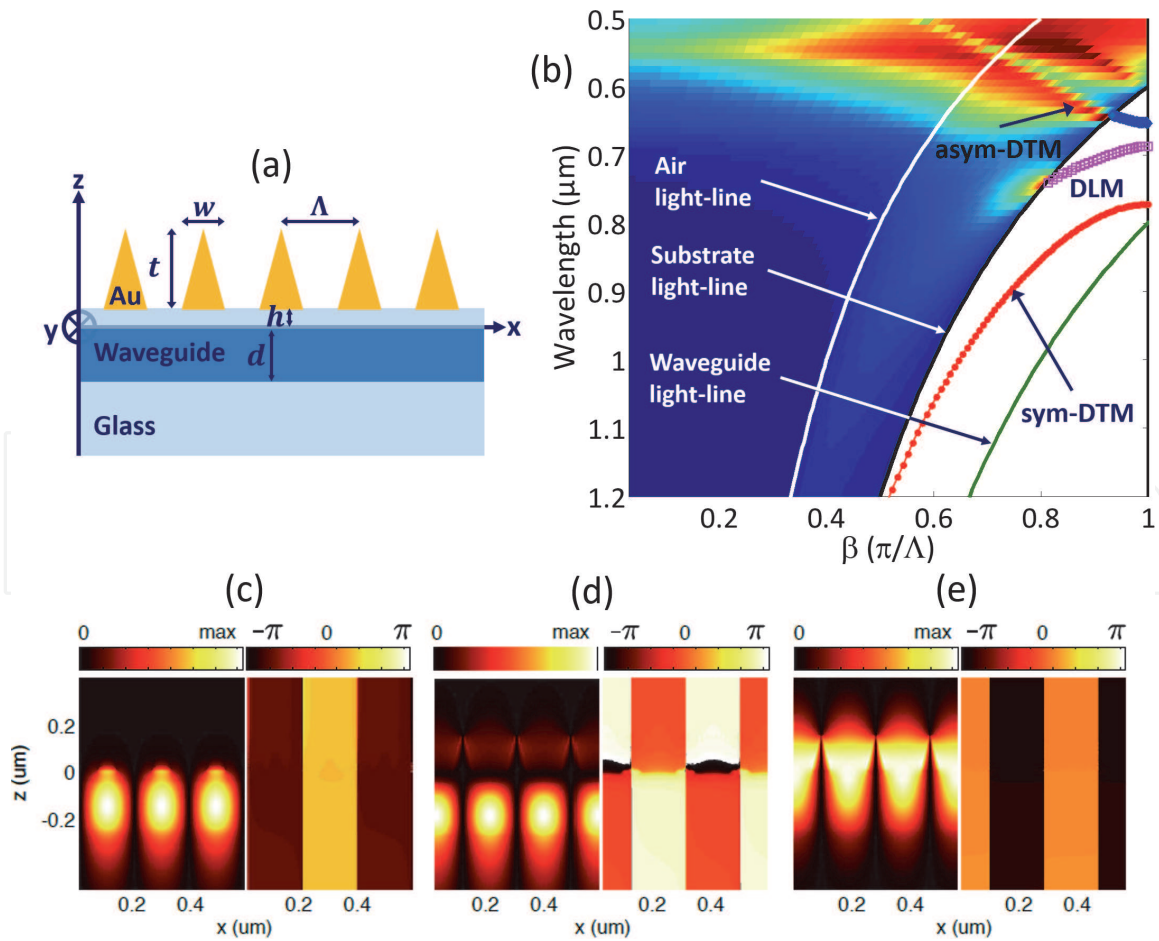


**Figure 14.**

(a) Schematic representation of an infinite periodic array of MNW integrated on top of a dielectric waveguide buried in a glass substrate. The superstrate is air. (b) In the dispersion curves are observed three chain modes in the guided region: DLM (magenta circles), asymmetric DTM (blue circles) and symmetric DTM (red dots). Distribution of the amplitude and phase of magnetic field in the out of plane direction of the (c) DLM, (d) asymmetric DTM and (e) symmetric DTM.

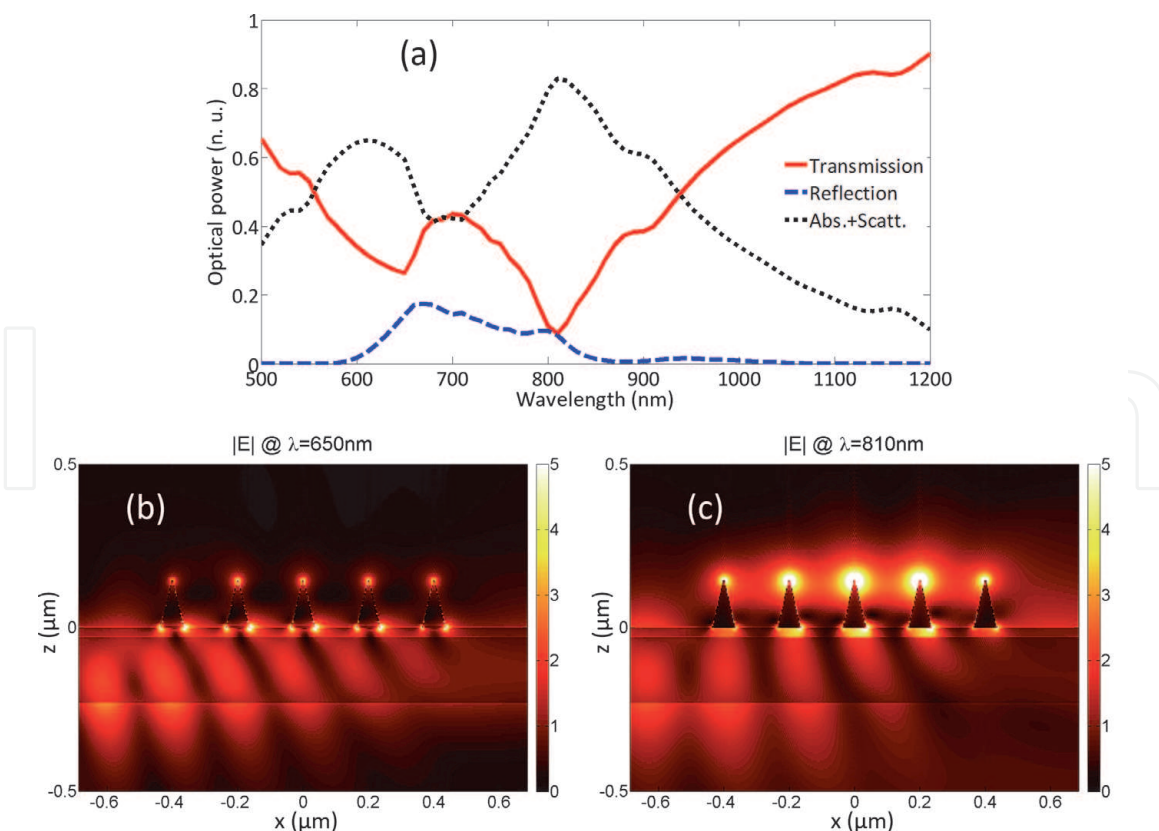


**Figure 15.**  
 (a) Normalized transmission (red), reflection (blue dashed) and absorption plus scattering (black dotted) curves of a periodic array of 5 gold nanowires integrated on top of the dielectric waveguide. (b) At  $\lambda = 650$  nm, the energy density map shows a field enhancement at the lower apices of the MNW. (c) At  $\lambda = 810$  nm, the energy density map shows a strong enhancement of the field at the upper apices of the MNW.

MNW with no phase difference between waveguide and MNW, being defined the symmetry of the modes.

To corroborate the coupling between the photonic and plasmonic chain modes, we simulated the beam propagation along the integrated structure. For this simulation, we used a finite number of 5 MNW and excited the waveguide with its fundamental  $TM_0$  mode. The transmission (red curve), reflection (blue dashed curve) and absorption plus scattering (black dotted curve) were normalized to the incident electromagnetic field and the results are shown on **Figure 15a**.

The transmission shows a first minimum value around  $\lambda = 650$  nm, corresponding to the excitation of DLM and antisymmetric DTM. This excitation is corroborated in the energy density map of **Figure 15b**, where is observed a field enhancement at the bottom apices of the nanowires. The second minimum observed in the transmission spectrum around  $\lambda = 810$  nm, correspond to the efficient excitation of the symmetric DTM, being characterized by a strong enhancement of the electromagnetic field at the upper apices of the nanowires, as can be observed in the energy density map of **Figure 15c**. According to the numerical calculations, at this wavelength the amplitude of the electromagnetic field measured 10 nm above the apex of the nanowires, is 8.7 times stronger in comparison to the amplitude of the incident electromagnetic field. This field enhancement is referred as tip-localized surface plasmon resonance.

## 4. Conclusions

As we have studied in this chapter, mode hybridization between plasmonic and photonic guided modes offers the possibility to design integrated devices for light



confinement in nanometric volumes. Also, as light propagates in dielectric structures, these integrated devices reduce intrinsic propagation losses in conventional plasmonic waveguides.

When properly excited, we have studied how localized surface plasmons can couple in periodic arrays of metallic nanowires, leading to light propagation. In other words, periodic arrays of MNW can behave as plasmonic waveguides. Depending on the geometry of their cross section (shape and aspect ratio), the electromagnetic field can be strongly confined and localized, desired property for number of applications, like excitation of quantum dots or single photon emitters, surface enhanced Raman spectroscopy, and biosensing.

The examples and explanations brought in this chapter can also be expanded to other geometries and material combinations. The reader should always remind that mode hybridization is the core of the physics behind the design of integrated photonic-plasmonic devices for light guiding applications.

These hybrid photonic-plasmonic systems offers the capability of matching diffraction limited guided optics, with nanometric materials, opening new perspectives for the development of a new generation of integrated optical devices.

## Acknowledgements

The authors thank National Council of Science and Technology, CONACYT, for partial financial support (Basic Scientific Research, Grant No. A1-S-21527).

## Conflict of interest

The authors declare no conflicts of interest.

## Author details


Ricardo Téllez-Limón<sup>1\*</sup> and Rafael Salas-Montiel<sup>2</sup>

1 CONACYT – Center for Scientific Research and Higher Education at Ensenada (CICESE), Unit Monterrey, Nuevo Leon, Mexico

2 L2n – Laboratory Light, Nanomaterials and Nanotechnologies, CNRS ERL 7004 and University of Technology at Troyes, Troyes, France

\*Address all correspondence to: rtellez@conacyt.mx; rafael.salas@utt.fr

## IntechOpen

© 2021 The Author(s). Licensee IntechOpen. This chapter is distributed under the terms of the Creative Commons Attribution License (<http://creativecommons.org/licenses/by/3.0>), which permits unrestricted use, distribution, and reproduction in any medium, provided the original work is properly cited. 

## References

- [1] Novotny L, Hecht B. Principles of Nano-Optics. 2nd ed. Cambridge: Cambridge University Press; 2012. 564 p. DOI: 10.1017/CBO9780511794193
- [2] Lévêque G, Martin, O. J. F. Optical interactions in a plasmonic particle coupled to a metallic film, *Optics Express*, 2006; 14:9971–9981. DOI: 10.1364/OE.14.009971
- [3] Dong, J-W, Deng, Z-L. Direct eigenmode analysis of plasmonic modes in metal nanoparticle chain with layered medium, *Optics Letters*, 2013; 38:2244–2246. DOI: 10.1364/OL.38.002244
- [4] Quinten M, Leitner A, Krenn J. R, Aussenegg F. R. Electromagnetic energy transport via linear chains of silver nanoparticles, *Optics Letters*, 1998; 23: 1331–1333. DOI: 10.1364/OL.23.001331
- [5] Brongersma M. L, Hartman J. W, Atwater H. A. Electromagnetic energy transfer and switching in nanoparticle chain arrays below the diffraction limit, *Physical Review B*, 2000; 62: R16356–R16359. DOI: 10.1103/PhysRevB.62. R16356
- [6] Fung K. H, Chan C. T. Plasmonic modes in periodic metal nanoparticle chains: a direct dynamic eigenmode analysis, *Optics Letters*, 2007; 32:973–975. DOI: 10.1364/OL.32.000973
- [7] Compaijen P. J, Malyshev V. A, Knoester J. Elliptically polarized modes for the unidirectional excitation of surface plasmon polaritons, *Optics Express*, 2016; 24:3858–3872. DOI: 10.1364/OE.24.003858
- [8] Février M, Gogol P, Aassime A, Mégy R, Delacour C, Chelnokov A, Apuzzo A, Blaize S, Lourtioz, J-M, Dagens B. Giant Coupling Effect between Metal Nanoparticle Chain and Optical Waveguide, *Nano Letters*, 2012; 12: 1032–1037. DOI: 10.1021/nl204265f
- [9] Saha S, Dutta A, Kinsey N, Kildishev A. V, Shalaev V. M, Boltasseva A. On-Chip Hybrid Photonic-Plasmonic Waveguides with Ultrathin Titanium Nitride Films, *ACS Photonics*, 2018; 5:4423–4431. DOI: 10.1021/acsphotonics.8b00885
- [10] Saleh B. E. A, Teich M. C. Fundamentals of Photonics. 2nd ed. New York: John Wiley & Sons, Inc; 2007. 947 p. DOI: 10.1002/0471213748
- [11] Maier S. A, Plasmonics: Fundamentals and Applications. New York: Springer US; 2007. 224 p. DOI: 10.1007/0-387-37825-1
- [12] Jackson J. D. Classical electrodynamics. 3rd ed. New York: Wiley; 1998. 832 p. ISBN: 9780471309321
- [13] Beltran Madrigal J, Tellez-Limon R, Gardillou F, Barbier D, Geng W, Couteau C, Salas-Montiel R, Blaize S. Hybrid integrated optical waveguides in glass for enhanced visible photoluminescence of nanoemitters, *Applied Optics*, 2016; 55:10263–10268. DOI: 10.1364/AO.55.010263
- [14] Tellez-Limon R, Blaize S, Gardillou F, Coello V, Salas-Montiel R. Excitation of surface plasmon polaritons in a gold nanoslab on ion-exchanged waveguide technology, *Applied Optics*, 2020; 59:572–578. DOI: 10.1364/AO.381915
- [15] Inclán Ladino A, Mendoza-Hernández J, Arroyo-Carrasco M. L, Salas-Montiel R, García-Méndez M, Coello V, Tellez-Limon R. Large depth of focus plasmonic metalenses based on Fresnel biprism, *AIP Advances*, 2020; 10: 045025. DOI: 10.1063/5.0004208
- [16] Katsidis C. C, Siapkias D. I. General transfer-matrix method for optical multilayer systems with coherent,

- p partially coherent, and incoherent interference,
- Applied Optics*
- , 2002; 41: 3978–3987. DOI: 10.1364/AO.41.003978
- [17] Anemogiannis E, Glytsis E. N. Multilayer waveguides: efficient numerical analysis of general structures, *Journal of Lightwave Technology*, 1992; 10:1344–1351. DOI: 10.1109/50.166774
- [18] Anemogiannis E, Glytsis E. N, Gaylord T. K. Determination of guided and leaky modes in lossless and lossy planar multilayer optical waveguides: reflection pole method and wavevector density method, *Journal of Lightwave Technology*, 1999; 17:929–941. DOI: 10.1109/50.762914
- [19] Kocabaş Ş. E, Veronis G, Miller D. A. B, Fan S. Modal analysis and coupling in metal-insulator-metal waveguides, *Physical Review B*, 2009; 79: 035120. DOI: 10.1103/PhysRevB.79.035120
- [20] Davis T. J. Surface plasmon modes in multi-layer thin-films, *Optics Communications*, 2009; 282:135–140. DOI: 10.1016/j.optcom.2008.09.043
- [21] Nesterov M. L, Kats A. V, Turitsyn S. K. Extremely short-length surface plasmon resonance devices, *Optics Express*, 2008; 16: 20227–20240. DOI: 10.1364/OE.16.020227
- [22] Kekatpure R. D, Hryciw A. C, Barnard E. S, Brongersma M. L. Solving dielectric and plasmonic waveguide dispersion relations on a pocket calculator, *Optics Express*, 2009; 17: 24112–24129. DOI: 10.1364/OE.17.024112
- [23] Haeseler F. V, Peitgen H. O. Newton's method and complex dynamical systems, *Acta Applicandae Mathematica*, 1988; 13:3–58. DOI: 10.1007/BF00047501
- [24] Garrido Alzar C. L, Martinez M. A. G, Nussenzeig P. Classical analog of electromagnetically induced transparency, *American Journal of Physics*; 2001; 70:37–41. DOI: 10.1119/1.1412644
- [25] Novotny L. Strong coupling, energy splitting, and level crossings: A classical perspective, *American Journal of Physics*, 2010; 78:1199–1202. DOI: 10.1119/1.3471177
- [26] Tellez-Limon R, Fevrier M, Apuzzo A, Salas-Montiel R, Blaize S. Modal analysis of LSP propagation in an integrated chain of gold nanowires. In: *Proceedings SPIE Nanophotonic Materials X*, 13 September 2013; San Diego. California: Proc. SPIE; 2013. p. 88070J
- [27] Tellez-Limon R, Fevrier M, Apuzzo A, Salas-Montiel R, Blaize S. Theoretical analysis of Bloch mode propagation in an integrated chain of gold nanowires, *Photonics Research*, 2014; 2:24–30. DOI: 10.1364/PRJ.2.000024
- [28] Tellez-Limon R, Février M, Apuzzo A, Salas-Montiel R, Blaize S. *Journal of the Optical Society of America B*, 2017; 34: 2147–2154. DOI: 10.1364/JOSAB.34.002147
- [29] Hocker G. B, Burns W. K. Mode dispersion in diffused channel waveguides by the effective index method, *Applied Optics*, 1977; 16:113–118. DOI: 10.1364/AO.16.000113
- [30] Payne F. P. A new theory of rectangular optical waveguides, *Optical and Quantum Electronics*, 1982; 14:525–537. DOI: 10.1007/BF00610308
- [31] Patchett S, Khorasaninejad M, Nixon O, Saini S. S. Effective index approximation for ordered silicon nanowire arrays, *Journal of the Optical Society of America B*, 2013; 30:306–313. DOI: 10.1364/JOSAB.30.000306
- [32] Szafranek D, Leviatan Y. A Source-Model Technique for analysis of wave guiding along chains of metallic

nanowires in layered media, *Optics Express*, 2011; 19:25397–25411. DOI: 10.1364/OE.19.025397

[33] Moharam M. G, Gaylord, T. K. Rigorous coupled-wave analysis of planar-grating diffraction, *Journal of the Optical Society of America*, 1981; 71: 811–818. DOI: 10.1364/JOSA.71.000811

[34] Moharam M. G, Grann E. B, Pommet D. A, Gaylord T. K. Formulation for stable and efficient implementation of the rigorous coupled-wave analysis of binary gratings, *Journal of the Optical Society of America A*, 1995; 12: 1068–1076. DOI: 10.1364/JOSAA.12.001068

[35] Liu H, Lalanne P. Comprehensive microscopic model of the extraordinary optical transmission, *Journal of the Optical Society of America A*, 2010; 27: 2542–2550. DOI: 10.1364/JOSAA.27.002542

[36] Noponen E, Turunen J. Eigenmode method for electromagnetic synthesis of diffractive elements with three-dimensional profiles, *Journal of the Optical Society of America A*, 1994; 11: 2494–2502. DOI: 10.1364/JOSAA.11.002494

[37] Li L. New formulation of the Fourier modal method for crossed surface-relief gratings, *Journal of the Optical Society of America A*, 1997; 14: 2758–2767. DOI: 10.1364/JOSAA.14.002758

[38] Kim H, Park J, Lee B. Fourier modal method and its applications in computational nanophotonics. 1<sup>st</sup> ed. Boca Raton: CRC Press; 2012. 326 p. DOI: 10.1201/b11710

[39] Bykov D. A, Bezus E. A, Doskolovich L. L. Use of aperiodic Fourier modal method for calculating complex-frequency eigenmodes of long-period photonic crystal slabs, *Optics Express*, 2017; 25: 27298–27309. DOI: 10.1364/OE.25.027298